Molecular Dynamics Study of Solvation of Coumarin-314 at the Water/Air Interface

Diego A. Pantano[†] and Daniel Laria*[,†,‡]

Departamento de Química Inorgánica, Analítica y Química-Física e INQUIMAE, Facultad de Ciencias Exactas y Naturales, Universidad de Buenos Aires Ciudad Universitaria, Pabellón II, 1428 Buenos Aires, Argentina, and Unidad Actividad Química, Comisión Nacional de Energía Atómica, Avenida Libertador 8250, 1429 Buenos Aires, Argentina

Received: May 30, 2002; In Final Form: December 12, 2002

Molecular dynamics experiments have been carried out to study equilibrium and dynamical aspects of orientational correlations and solvation of Coumarin-314 lying at the aqueous/air interface. Stable interfacial solvation states for the probe are characterized by an orientation of its molecular plane mostly parallel to the interface. At ambient temperature, spontaneous flipping transitions take place at characteristics time intervals of ≈0.5−1 ns; the pathway between the stable states involves a transition state in which the molecular dipole points perpendicularly to the interface. In-plane dynamics of the probe is characterized by a sequence of diffusive-like segments interrupted by the flipping episodes, whereas out-of-plane motions include large amplitude oscillations modulated by small-amplitude, fast rocking of the probe. Using nonequilibrium simulations, we also studied the solvation response of the surface following a vertical excitation of the probe. The overall solvation relaxation is slightly slower than that found in bulk, due to a lesser extent of rotational relaxation. Spatial characteristics of the surface solvation response is analyzed in terms of contributions from different individual solute−site responses. Dynamical results are also compared to predictions from linear theories.

I. Introduction

Liquid interfaces represent non-uniform environments where many chemical reactions of fundamental importance take place.[1−3] Equilibrium and dynamical characteristics of these reactions normally differ in a sensible way from those found in similar processes taking place in macroscopic condensed phases. The main reasons to account for such peculiarities are to be found in the large anisotropy of the force fields exerted on the liquid molecules in the close vicinity of the interface. These effects are translated into spatial and orientational correlations which are normally absent in conventional bulk phases that in turn affect the reactive channels in a nonsimple fashion.

In homogeneous environments, ultrafast time-resolved Stokes shift experiments are perhaps the most commonly used technique to gain direct information about the characteristics of the solvation dynamics.[4−7] Unfortunately, conventional time-resolved fluorescence experiments are not suitable for cases where it is required to probe molecular motions at interfaces, filtering out contributions from bulk species. Under these circumstances, nonlinear optical methods such as sum frequency generation[8] or second harmonic generation[9] (SHG) experiments emerge as more appropriate alternatives, since the signals are exclusively generated by probes adsorbed at the nonhomogeneous interface, with no interference from bulk species. These techniques have been successfully applied to the study of a variety of binary interfaces, including air/water,[10] quartz/water,[11] air/silica,[12] butanol/sapphire,[13] and to more complex structures, such as air/water interfaces containing amphiphilic molecules as well.[14]

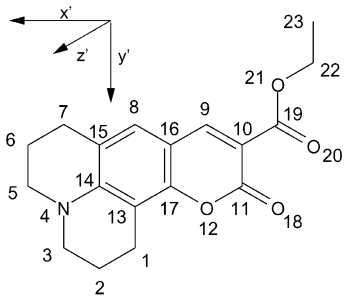

Figure 1. Coumarin-314.

In a series of recent papers,[15−18] Eisenthal and collaborators have investigated anisotropic orientational motion and solvation dynamics of Coumarin-314 (C-314) (Figure 1) adsorbed at the liquid/air interface. By a careful analysis of different signals generated from time-resolved pump and probe experiments they succeeded in determining solute orientational relaxations, discriminating out-of-plane from in-plane motions of photoexcited superficial C-314.[15] Moreover, they also measured solvation dynamics at the interface.[16−18] In this case, by varying the wavelength and the polarization state of the pump beam, they singled out responses of the interface for excited molecules exhibiting different degrees of solvation. Motivated by this body of experimental information, in the present paper we present microscopic details related to equilibrium and dynamic solvation of the same dye adsorbed at the water/air interface obtained from molecular dynamics experiments.

Computer simulations have been successfully implemented to unveil microscopic details of liquid interfaces.[19] More specifically, solvation dynamics at a series of water/nonpolar solvents has been investigated by Michael et al.[20] More closely related to the subject of the present paper, the behavior of simple

* Corresponding author. E-mail: dhlaria@cnea.gov.ar.
[†] Universidad de Buenos Aires Ciudad Universitaria.
[‡] Comisión Nacional de Energía Atómica.

10.1021/jp021306q CCC: $25.00
Published on Web 03/12/2003

ionic species at liquid/vapor interfaces has been analyzed by Benjamin.[21] One important conclusion of the latter study is the fact that, despite the structural differences exhibited by the interfaces, the collective polarization fluctuations that determine their responses, do not differ substantially from those prevailing in bulk phases. The present work extends the above-mentioned study, in an effort to incorporate a higher degree of molecular detail in the description of the solute so as to make closer contact with experimental results. In this way, we have extracted information that is inherently related to the particular geometry and charge distribution of the probe.

The remainder of this paper is organized as follows: In section II we provide details of the model and the methodology implemented in the simulation runs. Results for the equilibrium solvation are presented in section III. Section IV includes a microscopic analysis of the dynamical aspects of the solvation at the interface. The concluding remarks are presented in section V.

II. Model

We have performed molecular dynamics experiments on systems composed by a single C-314 lying at one of the liquid/air interfaces of an aqueous slab composed by $N_w = 800$ water molecules. The two interfaces were constructed by suppressing periodic boundary conditions along the *z*-axis in a previously equilibrated, fully periodic system; the volume of the original cell was $31.2 \times 31.2 \times 25.0$ Å^3. All molecules were modeled as rigid bodies containing a collection of interaction sites. The potential energy of the system was considered a sum of pairwise intermolecular interactions that included site−site Lennard-Jones and Coulomb interaction terms. The AM1 parametrization of the semiempirical AMPAC package[22] was used to determine the geometry and partial charges of the ground (S_0) and first excited (S_1) electronic states of the C-314 molecule. This level of approximation in the electronic structure calculation normally provides reasonable descriptions for the electronic densities of coumarin dyes.[23−26] Additional details of our calculations can be found in ref 26. The resulting C-314 dipole moments are $\mu_{S_0} = 8.4$ D and $\mu_{S_1} = 14.1$ D;[28] the value for the ground state is in reasonable agreement with experimental information,[27] whereas the excited-state value is slightly higher than that reported in ref 16. To describe the geometry and charge distribution of the water molecule, the simple point charge (SPC) model by Berendsen et al.[29] was adopted. All parameters for the solute and solvent interactions can be found in Table 1.

The dynamical trajectories corresponded to microcanonical runs at temperatures close to $T \approx 298$ K. In this temperature regime, the slab presented a stable structure, with negligible evaporation during the course of the simulations. After initial equilibration runs of typically ≈100 ps, statistics were collected along equilibrium trajectories lasting ≈2 ns. Nonequilibrium runs modeling a $S_0 \rightarrow S_1$ vertical transition were also performed. These trajectories included a previous equilibrium S_0 run using Nosé dynamics,[30] from which we selected initial conditions, separated by 1 ps intervals to provide statistically independent configurations. At $t = 0$, the thermostat was removed, the charges of the solute were set to their S_1 values, and particle velocities were assigned according to the Boltzmann distribution. From these initial conditions, we followed relevant observables during periods of 1 ps. To establish a comparison between interfacial and bulk solvation, we also performed a few test runs on fully periodic systems composed by C-314 dissolved in $N_w = 800$ waters at a density $\rho_w = 0.033$ Å^{-3}. The RATTLE algorithm[30] was employed to integrate the equations of motion with a time step of 1 fs. Intramolecular constraints were treated using the SHAKE algorithm.[30] All interactions where truncated at $R_c = 10.6$ Å and brought to zero in an interval of 1 Å by a fourth-degree spline.

TABLE 1: Potential Parameters

A. Water

site	s	e	q
O	3.17	0.156	−0.82
H	0.00	0.000	0.41

$d_{O-H} = 1.0$ Å; $d_{H-H} = 1.633$ Å

B. Coumarin-314

					c_α	
site	σ^a	ϵ^a	q_α	Δq_α	slab	bulk
C_1			−0.107	0.005	0.005	0.005
C_2			−0.167	0.003	0.004	0.004
C_3			−0.018	0.003	0.006	0.005
C_5			−0.017	0.003	0.005	0.004
C_6			−0.168	0.003	0.003	0.003
C_7			−0.111	0.005	0.005	0.005
C_8			−0.021	−0.062	0.009	−0.001
C_9			0.078	−0.257	0.590	0.588
C_{10}			−0.245	−0.018	0.044	0.040
C_{11}	3.50	0.080	0.357	−0.012	0.021	0.017
C_{13}			−0.185	0.086	0.087	0.085
C_{14}			0.186	−0.093	−0.147	−0.143
C_{15}			−0.168	0.080	0.079	0.088
C_{16}			−0.225	0.184	−0.153	−0.120
C_{17}			0.174	−0.073	0.021	0.009
C_{19}			0.359	−0.028	0.076	0.065
C_{22}			−0.009	0.000	0.000	0.000
C_{23}			−0.218	0.000	0.000	0.000
O_{12}			−0.198	−0.010	0.010	0.006
O_{18}			−0.261	0.019	−0.030	0.022
O_{20}	2.96	0.210	−0.322	−0.028	0.076	0.065
O_{21}			−0.297	−0.004	0.011	0.009
N_4	3.26	0.170	−0.272	0.140	0.274	0.275
H	2.50	0.005	0.14−0.21[b]	0.00−0.01[b]	0.04[c]	0.05[c]

[a] The Lennard Jones paramaters were considered the same for S_0 and the S_1 states. [b] The values represent the minimum and maximum values for q_H and Δq_H. [c] The values represent the sum of the different c_H. Length parameters are given in Å; energy parameters are given in kcal/mole; charge parameters are given in *e*. The usual geometrical and arithmetic means were used to determined the ϵ and σ parameters for the cross interactions.

III. Equilibrium Solvation

We will start our analysis by examining general aspects of the solvation structure of the ground state of the dye at the water/air interface. One of the gross features to consider is to determine the average location of the probe within the interface. Two useful quantities to consider in this connection are as follows: (i) the spatial correlation of the *z* coordinate of the center of mass of the coumarin with respect to the same coordinate of the water center of mass,

$$g_{C-CM}(z) = \langle \delta(Z_C - Z_{CM} - z) \rangle \tag{1}$$

and (ii) the number of water molecules per unit of area in the *x*−*y* plane, *A*, with their centers of mass lying between *z* and *z* + d*z* defined as

$$\rho_w(z) = \left\langle \frac{1}{A} \sum_{i=1}^{N_w} \delta(Z_i - Z_{CM} - z) \right\rangle \tag{2}$$

In the previous equations, $\langle ... \rangle$ denotes an equilibrium average while Z_C, Z_{CM}, and Z_i represent the *z*-coordinates of the centers

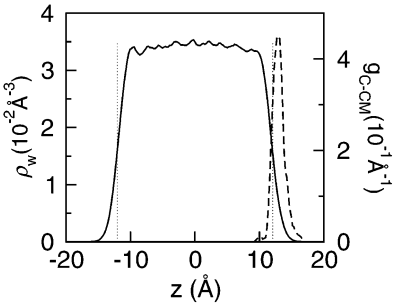

Figure 2. Local water density in the slab (solid line, left axis) and probability density for the center of mass of C-314 (dashed lines, righ axis) along the direction perpendicular to the interfaces. The dotted lines represent the locations of the two Gibbs dividing surfaces.

of mass of the C-314, the slab, and the *i*th water molecule, respectively. Results for the two spatial correlation functions are shown in Figure 2. The average width of the resulting slab measured between the two Gibss dividing surfaces was $\langle L \rangle = 25.1$ Å; the average local density at its central part was close $\langle \rho_w \rangle \approx 0.034$ Å^{-3}. We observe that the center of mass of the C-314 lies ≈1 Å outward from the Gibbs dividing surface located at $z = 12.2$ Å, with no significant degree of penetration into the bulk phase.

We also investigated orientational correlations of the probe at the interface. To facilitate our analysis, we found it convenient to define the primed local coordinate system shown in Figure 1. In this system, the dipole moment of the C-314 in the S_0 electronic state lies practically on the $z' = 0$ plane and makes an angle of 18° with the x' direction; for the S_1 state, the dipole moment roughly coincides with the x'-axis. The direct inspection of a large number of configurations revealed that the molecular $z' = 0$ plane of the coumarin remains mostly parallel to the interface. A snapshot of such a typical configuration is shown in Figure 3a. In Figure 4 we include details of the time evolutions of several orientational parameters along a 2 ns trajectory. The top panel displays results for $\cos \theta'(t) = \hat{\boldsymbol{z}}'(t) \cdot \hat{\boldsymbol{z}}$; where $\hat{\boldsymbol{z}}$ represents a unit vector in the *z*-direction. It is clear that most of the time, the stable superficial states of the probe are characterized by $\cos \theta' \approx \pm 1$, corroborating the above-mentioned observation. Flipping transitions between these stable states take place on a characteristic time scale of $\tau_{flp} \sim 0.5-1$ ns, revealing the presence of an activation free energy barrier, ΔF, intermediate between ≈5 and 10 k_BT, that prevents frequent transitions between the two stable solvation states.[31]

Additional details about the mechanism that drives the coumarin flip at the interface can be obtained from the analysis of the temporal evolution of the out-of-plane dynamics of the probe expressed in terms of $\cos \theta(t) = \hat{\mu}(t) \cdot \hat{z}$, shown in the middle panel of Figure 4. Note that all successful transition episodes are correlated with those in which the dipole raises practically perpendicular to the interface, with a preferential solvation of the negative charge end of the molecule (see Figure 3b). Nevertheless, this preferential orientation seems to be a necessary, albeit not sufficient, requirement for the molecular flip to occur, since many aborted rotations are also characterized by $\cos \theta > 0.5$. Confirmation of this hypothesis would certainly require a more detailed analysis of trajectories originated at different transition states;[32] at this point, we do not discard the possibility that the reaction coordinate for the C-314 rotation at the interface not only does involve orientational degrees of freedom of the probe but, most likely, a subset of the solvent degrees of freedom as well.

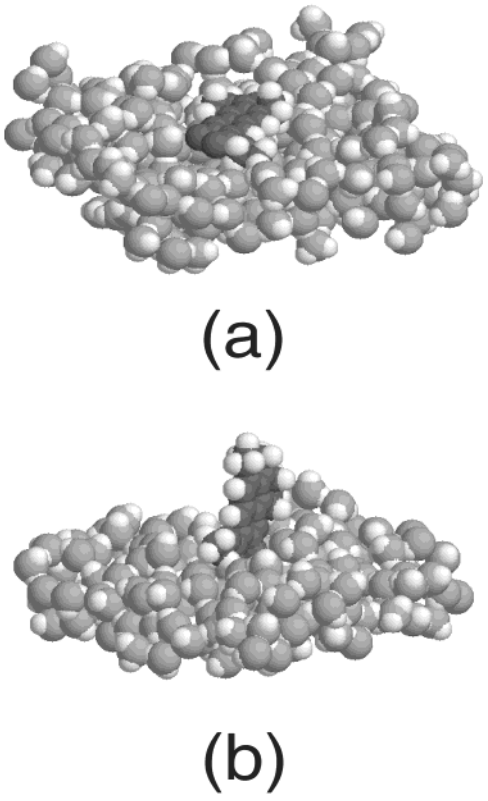

Figure 3. Snapshots for two configurations for C-314 at the interface: (a) Stable solvation state; (b) intermediate state for the molecular flip (see text). For clarity purposes only the first two water layers in the vicinity of the interface are displayed.

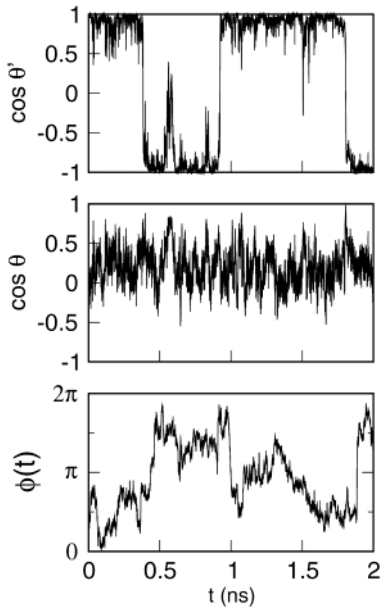

Figure 4. Time evolution of the orientational parameters for C-314 at the inteface: (top panel) $\cos \theta'$ (see text); (middle panel) out-of-plane orientation $\cos \theta$; (bottom panel) in-plane orientation $\phi(t)$.

IV. Dynamical Results

A. Orientational Dynamics. Experimental information about the orientational correlations of interfacial C-314 relevant in the present context can be summarized as follows:[15] (i) using null angle techniques, the most probable out-of-plane orientation of the C-314 was found to be $\theta \approx 80°$;[33] (ii) the reported time constants for the relaxations of the out-of-plane and in-plane

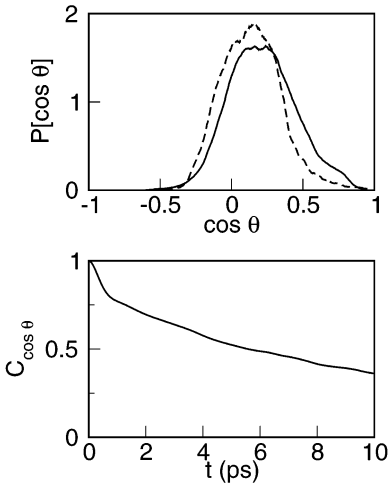

Figure 5. (Top panel) probability density for the out-of_plane orientation; (bottom panel) equilibrium time correlation function for the out-of-plane orientational parameter.

dynamics are $\tau_{\text{out}} = 350 \pm 20$ ps and $\tau_{in} = 600 \pm 40$ ps, respectively.

An analysis of some of these quantities can be carried out from the equilibrium simulation results depicted in Figures 4 and 5. In the top panel of Figure 5 we present results for the distribution $P[\cos\theta]$:

$$P[\cos\theta_0] = \langle\delta[\cos\theta - \cos\theta_0]\rangle \tag{3}$$

for the ground and first excited electronic states. We observe that both profiles present broad distributions shifted toward the positive axis, being the most probable orientations $\bar{\theta}_g = 79°$ and $\bar{\theta}_e = 82°$, in excellent agreement with the experimental measurements. The larger magnitude of the dipole moment for the S_1 electronic state—and, consequently, the stronger coumarin−interface coupling—explains the observed shift and narrowing of the distribution for the latter case. However, considering the small variations in $\bar{\theta}$, instead of analyzing orientational relaxation upon an excitation of the probe, we found it more convenient to perform our dynamical analysis from an equilibrium−time−correlation-function perspective.

The bottom panel of Figure 5 includes results for the temporal correlation for the out-of-plane motion defined as

$$C_{\cos\theta}(t) = \frac{\langle\delta[\cos\theta(t)]\,\delta[\cos\theta(0)]\rangle}{\langle(\delta[\cos\theta])^2\rangle} \tag{4}$$

where $\delta O(t) = O(t) - \langle O\rangle$. The decay of $C_{\cos\theta}(t)$ in the time interval considered presents a bimodal character: An initial decay lasting on the order of ≈0.5 ps involving ≈20% of the total relaxation, followed by a much slowly variant tail, characterized by a time scale of 15−20 ps. Our physical interpretation of these two time domains is as follows: The early stages of the correlation corresponds to small amplitude, fast rockings clearly perceptible in the time evolution depicted in the middle panel of Figure 4, whereas the long time tail can be ascribed to the less frequent, larger amplitude attempts, where $\cos\theta$ surpasses, for example, 0.6−0.7.

The bottom panel of Figure 4 present results for the evolution of the in-plane dynamics described in terms of $\phi(t) = \cos^{-1}[\hat{x}'\cdot\hat{\mu}_{||}(t)]$, where $\hat{\mu}_{||}(t)$ represents the instantaneous projection of the C-314 dipole moment in the $x-y$ plane. The overall description of the dynamics is somewhat more complex: At a first glance, the time evolution of $\phi(t)$ can be described in terms

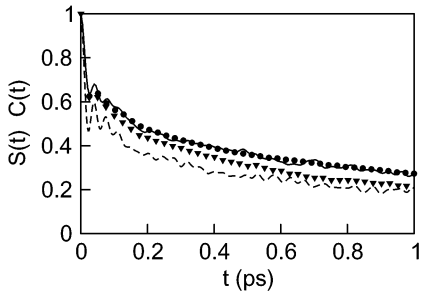

Figure 6. Solvation responses for C-314: (solid lines) superficial solvation; (dashed line) bulk solvation. Also shown are the equilibrium time correlation functions $C(t)$ for the ground (circles) and first electronic excited state (triangles) of the probe.

of a sequence of diffusive paths, characterized by fast fluctuations which are the consequence of the continuous buffeting produced by the water molecules lying at the interface. These time segments are interrupted by sudden jumps coinciding with the molecular flips. The physical picture that emerges from these results suggests that during the latter episodes the coumarin sticks out from the aqueous phase, the surface friction decreases drastically and the molecule performs an almost-free, in-plane rotation, before "landing back" on the interface. The time evolution of $\phi(r)$ shows that the C-314 performs a full in-plane rotation in characteristic time intervals lasting several hundreds of picoseconds; given the length of our simulation experiments, time scales in that range are of difficult computation. Anyhow, for the sake of comparison, one can estimate the period for C-314 considered as a free rotor: $\tau_{\text{free}} \propto \sqrt{I_{z'}/k_B T} \approx 5$ ps, where $I_{z'}$ is the principal moment of inertia of the coumarin along z'. The large disparity between this time scale and that of the observed dynamics, along with the fact that the coumarin lies mostly flat on the surface, confirm the role of superficial friction as a leading controlling agent for the in-plane rotational dynamics.

B. Solvation Dynamics. The next step in our analysis will be the description of the response of the aqueous interface following a vertical excitation of the probe. In simulation studies, the usual way to tackle the problem is by considering the normalized nonequilibrium response defined by

$$S(t) = \frac{\langle E(t) - E(\infty)\rangle_{ne}}{\langle E(0) - E(\infty)\rangle_{ne}} \tag{5}$$

in the previous equation, $\langle ...\rangle_{ne}$ denotes an average taken from a distribution of nonequilibrium initial configurations.[36] $E(t)$ is the instantaneous Coulombic energy gap defined as[7,26]

$$E(t) = \sum_{\alpha} E_{\alpha}(t) = \sum_{\alpha} \Delta q_{\alpha} V_{\alpha}(t) \tag{6}$$

where Δq_{α} and $V_{\alpha}(t)$ represent the charge jump due to the electronic excitation and the instantaneous solvent electrical potential at the α-site of C-314 at time t, respectively.

In Figure 6 we present results for the solvation relaxations for superficial and bulk solvation of the probe. Both curves present similar features, being the overall relaxation in bulk slightly faster. The observed difference is mainly due to a more pronounced relaxation of the bulk curve during the first ≈50 fs. This portion of the relaxation is normally ascribed to small-amplitude librations of the solvent, so our results indicate that, in bulk, these motions account for a larger fraction of the total relaxation: 50 vs 35%, in the case of interfacial solvation. A

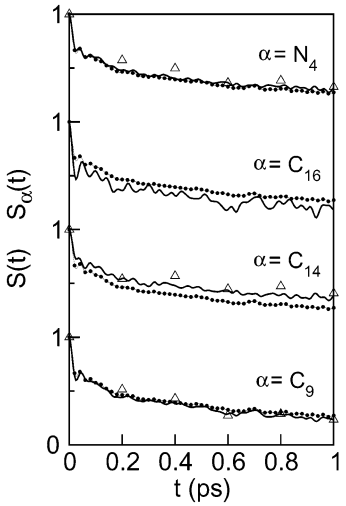

Figure 7. Solvation responses at selected C-314 sites (solid lines). The dots represent the overall solvation responses. The triangles represent relaxations of the populations $N_H(t)$ (see text).

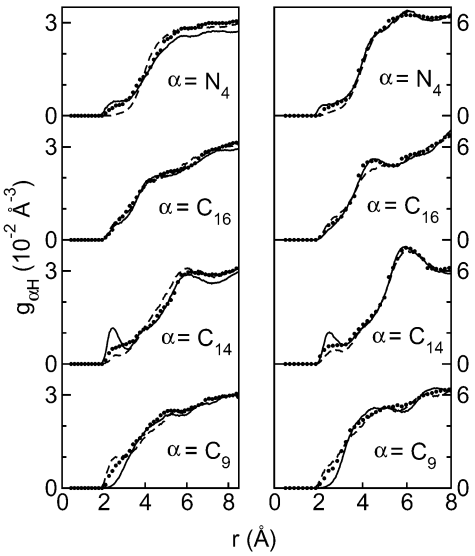

Figure 8. Site−site pair correlation functions $g_{\alpha,H}(r)$ for surface solvation (left panel) and bulk solvation (righ panel) of C-314: (solid lines) S_0; (dashed lines) S_1. Also shown are transients for the density fields at $t = 1$ ps (circles).

crude order of magnitude for the overall characteristic time of the solvation, τ_s, can be obtained from the integral

$$\tau_s = \int_0^\infty S(t)\, dt \tag{7}$$

Simulation results for interfacial and bulk solvation in SPC water are $\tau_s^{int} \approx 0.79$ ps and $\tau_s^{blk} \approx 0.56$ ps, respectively. Note that these values compare well and present the correct trend exhibited by the slowest relaxation times found in the TRSH experiments:[16−18,34] $\tau_s^{int} \approx 0.82-1.2$ ps (depending on the polarization of the pump beam considered) and $\tau_s^{blk} \approx 0.69-0.88$ ps.[35] For systems interacting via site−site potentials, the overall solvation response of a given environment can be conveniently decomposed in contributions from different solute-site responses $S_\alpha(t)$ according to[26]

$$S(t) = \sum_\alpha c_\alpha S_\alpha(t) \tag{8}$$

where the coefficient c_α represents the fractional contribution of site α to the total Coulomb energy gap, namely,

$$c_\alpha = \frac{\langle E_\alpha(0) - E_\alpha(\infty)\rangle_{ne}}{\langle E(0) - E(\infty)\rangle_{ne}} \tag{9}$$

S_α is defined as

$$S_\alpha(t) = \frac{\langle E_\alpha(t) - E_\alpha(\infty)\rangle_{ne}}{\langle E_\alpha(0) - E_\alpha(\infty)\rangle_{ne}} \tag{10}$$

Results for the set of c_α for surface and bulk environments are presented in the last two columns of Table 1, while a few selected site responses are depicted in Figure 7. Several observations related to these results are worth commenting on: (i) the nonequilibrium response is predominantly dominated by the solvent responses for four sites, namely, C_9, N_4, C_{14}, and C_{16}; (ii) bulk and superficial solvation present practically identical values of c_α; (iii) expressed in terms of their individual weights, certain solute sites, including the last two mentioned C_{14} and C_{16}, present negative contributions to the total relaxation, a simple physical interpretation of these results can be rationalized if one realizes that these two tagged sites lie close to N_4 and C_9; the observed "frustrated" site solvations are due to the characteristics of the local electric fields provided by the interface in the vicinity of those sites, which are not sufficiently quickly variant in space to simultaneously stabilize sites exhibiting Δq_α with opposite signs; (iv) the temporal evolutions of the most prominent individual site relaxations investigated are described by similar time scales to that governing the overall response. This would confirm that the latter is the result of large cancellations from different site contributions with similar temporal characteristics.

In bulk phases, the long-time portion of the solvation relaxation is normally associated with diffusive dynamics of the environment. To gain additional insight about the characteristics of these motions, one can monitor the time evolution of different solvent density fields in the close vicinity of the solute. For this particular case, we found that the clearest results are those extracted from transients of spatial correlations involving H-sites in the solvent. In Figure 8 we present results for relevant $g_{\alpha H}(r;t)$, defined as

$$g_{\alpha H}(r;t) = \frac{1}{4\pi r^2}\left\langle \sum_i^{N_w} \delta(|\mathbf{r}_\alpha(t) - \mathbf{r}^H{}_i(t)| - r)\right\rangle \tag{11}$$

where $\mathbf{r}_\alpha(t)$ and $\mathbf{r}^H{}_i(t)$ represent the coordinate of site α in C-314 and the H-site of the ith water molecule at time t, respectively. The figure contains equilibrium results for bulk and superficial solvation corresponding to $t = 0$ and $t = \infty$, and a nonequilibrium transient profile computed at $t = 1$ ps as well. The variety of intramolecular length scales characterizing the geometry of the probe, all of them of comparable size, lead to rather featureless profiles. Moreover, apart from the obvious differences in a factor 2, the solvation structures at the interface look practically identical to those in bulk. Interestingly, the inspection of these profiles confirms the aforementioned "frustrated" site solvation of sites C_{14} and C_{16}. The case of the former site is perhaps the most evident: Note that despite the fact that Δq_{C14} is negative, the $t = 0$ hydrogen peak at $r \approx 2.4$ Å gradually vanishes. These situations should be contrasted with the "standard" behavior of the curves for N_4, which exhibit the opposite trend. As a confirmation of the diffusive character of

the last portion of the relaxation, in Figure 7 we also present results of the relaxation of the population of solvent hydrogen sites, described in terms of the following quantity:

$$S_N^{\alpha}(t) = \frac{\langle N_H^{\alpha}(t) - N_H^{\alpha}(\infty)\rangle_{ne}}{\langle N_H^{\alpha}(0) - N_H^{\alpha}(\infty)\rangle_{ne}} \quad (12)$$

In the previous equation, $N_H^{\alpha}(t)$ represents the number of solvent H-sites lying at a distance smaller than a threshold value—arbitrarily set at 3 Å— from the solute site α. With the exception of C_{16}, where changes in the hydrogen density field are unpercetible, the good agreement between the decays of $S_N^{\alpha}(t)$ and $S_{\alpha}(t)$ is clear evidence of the diffusive character of the second portion of the responses.

Before closing this section, we will comment on a last aspect dealing with the validity of linear response theories (LRT) as a predictive tool for estimating nonequilibrium relaxations. The fluctuation−dissipation theorem states that for sufficiently small perturbations, the overall interfacial relaxation can be reasonably well-described in the following terms:[36]

$$S(t) \approx C(t) = \frac{\langle \delta E(t)\, \delta E(0)\rangle}{\langle (\delta E)^2\rangle} \quad (13)$$

where $\delta E(t) = E(t) - \langle E\rangle$ represents spontaneous fluctuations of the interface energy gap. Results for the equilibrium time correlation functions for the ground and first excited electronic states are presented in Figure 6. Interestingly, despite the complexities found in the microscopic interpretation of the overall solvation response, LRT maintains an excellent predictive power regardless the Born−Oppenheimer potential energy surface chosen to describe the equilibrium dynamics.

V. Concluding Remarks

The results presented in this paper provide new insights on superficial states of polyatomic probes at liquid/air interfaces. The main goal of the study was to go beyond simplified models, incorporating a higher level of geometrical details in the description of the electronic distributions of the solute in the ground and first excited electronic states. With this more elaborated Hamiltonian, not only did we succeed in reconstructing the actual scenario that prevails at water/air interfaces but also we provided microscopic interpretations for several phenomena probed by nonlinear spectroscopy experiments. In this way, we were able to extract information about the nature of the orientational dynamics at the interfaces, the characteristic time scales that govern these motions, and how the solvent dynamics is affected by the asymmetries imposed by the presence of a free surface. We know no previous simulation studies on solvation dynamics at interfaces that have been performed at this level of molecular detail. Our simulations show that stable solvation states of C-314 are characterized by flat orientations of its molecular plane along the interface. Out-of-plane orientational distributions for the ground and first electronic states are both characterized by a variety of orientations—ranging from typically $\cos\theta \sim -0.1$ up to $\cos\theta \sim 0.5$—with averages values $\bar{\theta}$ close to 80°.

From the dynamical point of view, the overall dynamics of the probe has been described in terms of in-plane and out-of-plane motions. The former is characterized by slow diffusive segments interrupted by sudden jumps, correlated with episodes in which the coumarin flips over the surface. On the other hand, the out-of-plane dynamics is characterized by large-amplitude rotations, taking place at time scales of a few tens of picoseconds, modulated with a much faster, smaller amplitude rocking motions. In addition, flipping episodes seem to be triggered by large-amplitude out-of-plane motions, during which the molecule pivots, keeping the negatively charged end of its dipole buried into the aqueous phase. Similar mechanisms have been suggested for the interpretation of the faster rate constants for the isomerization process of superficial carbocyanines;[37] in this case, the penetration into the gas phase would lead to a reduction of the friction provided by the interface, speeding up the isomerization process.

Despite the rather complex charge distribution of the C-314—compared, for example, to the case of simple ionic species—the overall solvation response of the interface still looks similar to that found in bulk water, confirming direct experimental findings.[17,18] The characteristic times and the observed trends for bulk and interfacial solvation obtained from our simulations compare reasonably well with results from nonlinear optics experiments. The decomposition of the response into contributions from different sites provided information about the nature of the spatial characteristics of the suceptibility of the interface. Our results show that the response of the interface is predominantly dominated by two pairs of site contributions, each one comprising sites with opposite Δq_{α}. Similar features have been observed in simulations of coumarins attached to polar clusters.[26] Regardless this nontrivial interplay between contributions from different solute sites, linear theories still provide excellent descriptions of the overall superficial and bulk responses. We tend to believe that the reasons for this remarkable performance should be found in the large cancellations between the observed nonlinearities.

Acknowledgment. D.L. is a staff member of CONICET (Argentina).

Supporting Information Available: Table S1, giving full description of the different solute coordinates and charges. This material is available free of charge via the Internet at http://pubs.acs.org

References and Notes

(1) For recent review articles see, for example:, Benjamin, I. *Chem. Rev.* **1996**, *96*, 1449. Benjamin, I. *Annu. Rev. Phys. Chem.* **1997**, *48*, 407. Benjamin, I. *Acc. Chem. Res.* **1995**, *28*, 233.

(2) Eisenthal, K. *Annu. Rev. Phys. Chem.* **1992**, *43*, 627.

(3) Adamson, A. W. *Physical Chemistry of Surfaces*; Willey: New York, 1990.

(4) Maroncelli, M. *J. Mol. Liq.* **1993**, *57*, 1.

(5) (a) Maroncelli, M.; Kumar, P. V.; Papazyan, A.; Horng, M. L.; Rosenthal, S. J.; Fleming, G. R. In *Ultrafast Reaction Dynamics and Solvent Effects*; Gaudel, Y., Rossky, P. J., Eds.; American Institute of Physics: New York, 1994.

(6) Fleming, G. R. *Chemical Applications of Ultrafast Spectroscopy*; Oxford University Press: New York, 1986.

(7) Kumar, P. V.; Maroncelli, M. *J. Chem. Phys.* **1995**, *103*, 3038. Reynolds, L.; Gardecki, J. A.; Frankland, S. J. V.; Horng, M. L.; Maroncelli, M. *J. Phys. Chem.* **1996**, *100*, 10337.

(8) Shen, Y. R. *The Principle of Nolinear Optics*; Wiley: New York, 1984. Shen, Y. R. *Annu. Rev. Phys. Chem.* **1989**, *40*, 327.

(9) Heinz, T. F. In *Nonlinear Surface Electromagnetic Phenomena*; Ponath, H., Stegeman, G., Eds.; Elsevier: Amsterdam, 1991. Bervet, P. F.; Girault, H. H. *Second Harmonic Generation at Liquid/Liquid Interfaces*; CRC Press: Boca Raton, FL, 1996. Eisenthal, K. B. *Acc. Chem. Res.* **1993**, *26*, 636.

(10) Bhattacharyya, K.; Sittzmann, E. V.; Eisenthal, K. B. *J. Phys. Chem.* **1988**, *87*, 1442.

(11) Meech, S. R.; Yoshihara, K. J. *J. Phys. Chem.* **1990**, *94*, 4913. Ong, S.; Zhao, X.; Eisenthal, K. B. *Chem. Phys. Lett.* **1992**, *191*, 327.

(12) Morgenthaler, M. J. E.; Meech, S. R. *J. Phys. Chem.* **1996**, *100*, 3323. Heinz, T. F.; Tom, H. W. K.; Shen, Y. R. *Phys. Rev. A* **1983**, *28*, 1983.

(13) Yanagimachi, M.; Tamai, N.; Mahuhara, H. *Chem. Phys. Lett.* **1993**, *201*, 115.
(14) Benderskii, A. V.; Eisenthal, K. B. *J. Phys. Chem. B* **2000**, *103*, 11723. Benderskii, A. V.; Eisenthal, K. B. *J. Phys. Chem. B* **2001**, *105*, 6698.
(15) Zimdars, D.; Dadap, J. I.; Eisenthal, K. B.; Heinz, T. F. *J. Phys. Chem. B* **1999**, *103*, 3425.
(16) Zimdars, D. J.; Dadap, I.; Eisenthal, K. B.; Heinz, T. F. *Chem. Phys. Lett.* **1999**, *301*, 112.
(17) Zimdars, D.; Eisenthal, K. B. *J. Phys. Chem. A* **1999**, *103*, 10567.
(18) Zimdars, D.; Eisenthal, K. B. *J. Phys. Chem. B* **2001**, *105*, 3393.
(19) See ref 1 and references therein.
(20) Michael, D.; Benjamin, I. *J. Chem. Phys.* **2001**, *114*, 2817.
(21) Benjamin, I. *J. Chem. Phys.* **1991**, *95*, 3698.
(22) AMSOL 5.4.1. Hopkins, G. D. *AMPAC 5.0*; Semichem Inc. and Oxford Univesity Press: Shawnee, KS, and New York, 1986.
(23) McCarthy, P. K.; Blanchard, G. J. *J. Phys. Chem.* **1993**, *97*, 12205.
(24) Rechthaler, K.; Köhler, G. *Chem. Phys.* **1994**, *189*, 99.
(25) A parametrization similar to that used in the present study was employed in ref 7.
(26) Tamashiro, A.; Rodriguez, J.; Laria, D. *J. Phys. Chem.* **2002**, *106*, 215.
(27) Moylan, C. R. *J. Phys. Chem.* **1994**, *98*, 13513.
(28) The structures shown in Figure 1 and that shown in ref 16 are practically isoenergetic (within ≃1 kcal/mol) and differ in a rotation of the dihedral angle along the $O_{21}–C_{22}$ bond; the one presented here yields a closer agreeement with the experimental dipolar moment reported in ref 27.
(29) Berendsen, H. J. C.; Postma, J. P. M.; Von Gunsteren, W. F.; Hermans, J. *Intermolecular Forces*. Reidel: Dordrecht, The Netherlands, 1981.
(30) Allen M. P.; Tildesley, D. J. *Computer Simulation of Liquids*; Clarendon: Oxford, U.K., 1987.
(31) From the characteristics time for the transition, τ, and using standard transition-state theory arguments, a rough estimate of the free energy barrier can be obtained from $\Delta F \approx k_B T \ln(\tau/\tau_0)$, where τ_0 is a characteristic time for the microscopic processes, typically ≈1 ps.
(32) Methods based on statistical sampling of transition pathways may be appropriate to determine the reaction coordinate. For a detailed discussion, see: Bolhius, P. G.; Dellago, C.; Chandler, D.; Geissler, P. *Ann. Rev. Phys. Chem.* **2002**, *53*, 291.
(33) The local coordinate system reported in ref 15 is slightly different from that adopted here. In particular, cos θ is measured with respect to the ζ direction, taken along the molecular transition dipole moment. Still, we believe that this difference should not preclude a direct comparison between simulation and SHG results.
(34) The relaxations present a bimodal character with initial decays lasting ≃200−300 fs.
(35) These values are also comparable to the relaxation time for the structurally similar Coumarin-343 in bulk water; see: Walker, G. C.; Harzeb, W.; Kang, T. J.; Johnson, A. W.; Barbara, P. F. *J. Opt. Soc. Am. B* **1990**, *7*, 1521. Jimenez, R.; Fleming, G.; Kumar, P.; Maroncelli, M. *Nature* **1994**, *369*, 471.
(36) Chandler, D. *An Introduction to Modern Statistical Mechanics*; Oxford University Press: New York, 1987; Chapter 8.
(37) Sitzmann, E. V.; Eisenthal, K. B. *J. Phys. Chem.* **1988**, *92*, 4579.